

# Colossal and tunable dielectric tunability in domain-engineered barium strontium titanate

Received: 4 May 2025

Accepted: 20 August 2025

Published online: 26 September 2025

 Check for updates

Dongfang Chen<sup>1</sup>, Sergey Nisnevich<sup>2</sup>, Liyan Wu<sup>1</sup>, Zongquan Gu<sup>1</sup>, John Carroll<sup>3,4</sup>, Yizhe Jiang<sup>5</sup>, Cedric J. G. Meyers<sup>1</sup>, Kathleen Coleman<sup>6</sup>, Brendan M. Hanrahan<sup>6</sup>, Lane W. Martin<sup>7</sup>, Ilya Grinberg<sup>8</sup> & Jonathan E. Spanier<sup>1,2,3,9</sup>✉

Realization of tunable materials that are multifunctional and maintain high performance in dynamically changing environments is a fundamental goal of science and engineering. Tunable dielectrics form the basis of a wide variety of communication and sensing devices and require breakthrough performance improvement to enable next-generation technologies. Using phenomenological modeling, film growth, and characterization, we show that devices consisting of domain-wall-rich  $\text{Ba}_{0.8}\text{Sr}_{0.2}\text{TiO}_3$  films close to a polar-domain-variant phase boundary exhibit colossal dielectric tunability of 100:1 (99%) at a voltage (electric field) of  $\sim 15$  V (750 kV/cm), resulting in a tunability-quality factor product figure of merit that rises to nearly  $10^5$ , two orders of magnitude higher than the best previous reported values. Remarkably, varying the amplitude of alternating-current bias enables modulation of this tunability by 50%, owing to domain-wall motion. These results suggest that domain engineering is a powerful approach for achieving excellent modulation of functional properties in ferroelectric films.

With the increase in renewable energy generation and adoption of the electric vehicle (EV) charging, power grids face increasing challenges in balancing supply and demand<sup>1–3</sup>. This leads to a need for continuous non-contact monitoring of direct current (DC) power via electric field sensing of the grid and the growing number of DC power storage units and microgrids. One electric field sensor was proposed based on changing capacitance via varactors, which would not require moving components and allow for continuous monitoring at DC and low frequencies<sup>4</sup>. The performance of these sensors relies on the tunability of low frequency varactors, which to date have largely been limited to

p-n junction-based varactors. With the need for higher sensitivity, materials with high dielectric tunability are desired.

Since their discovery in the 1940s, ferroelectric perovskites based on  $\text{BaTiO}_3$  solid solutions have been widely used as dielectrics, motivating long-standing research interest both in academia and industry. The tunability of the dielectric constant ( $\epsilon$ ) by the application of electric bias ( $d\epsilon/dE$ ) is an important property because it enables frequency-agile dielectrics vital for low frequency tunable varactors for electric field sensors and power monitoring. Additionally, these could be used in other applications such as tunable phase shifters, antennas, filters, and

<sup>1</sup>Department of Mechanical Engineering & Mechanics, Drexel University, Philadelphia, PA 19104-2875, USA. <sup>2</sup>Department of Physics, Drexel University, Philadelphia, PA 19104-2875, USA. <sup>3</sup>Department of Electrical & Computer Engineering, Drexel University, Philadelphia, PA 19104-2875, USA. <sup>4</sup>DEVCOM, C5ISR Center, Army Futures Command, Aberdeen Proving Ground, Aberdeen, MD 21005-5066, USA. <sup>5</sup>Department of Materials Science & Engineering, University of California at Berkeley, Berkeley, CA 94720-1760, USA. <sup>6</sup>DEVCOM, U.S. Army Research Laboratory, Adelphi, MD 20783-1197, USA. <sup>7</sup>Department of Materials Science and NanoEngineering, Chemistry, and Physics and Astronomy, and Rice Advanced Materials Institute, Rice University, Houston, TX 77005, USA. <sup>8</sup>Department of Chemistry, Bar Ilan University, Ramat Gan 52900, Israel. <sup>9</sup>Department of Materials Science & Engineering, Drexel University, Philadelphia, PA 19104-2875, USA. ✉e-mail: [spanier@drexel.edu](mailto:spanier@drexel.edu)

oscillators<sup>5–7</sup>. The effect of the presence of polar domains (i.e., regions of the material with different orientations of polarization common in ferroelectrics) on materials for such applications can vary, with both beneficial and detrimental effects reported<sup>8–12</sup>. Recent research has shown that strain-driven phase transitions between domain-variant phase boundaries can be used to achieve high values of dielectric constant<sup>13</sup>. Application of an electric field that shifts the material away from the domain-variant phase boundary, therefore, provides an effective knob to dramatically decrease the dielectric constant with increasing field, leading to the high tunability sought for such applications. At the same time, current materials that exhibit large dielectric tunability and their use in the above applications are constrained by the inability to dynamically control or modulate the tunability.

Ba<sub>1-x</sub>Sr<sub>x</sub>TiO<sub>3</sub> (BST) solid solutions have formed the core of frequency-agile devices due to their superior combination of high dielectric constant, high tunability and low dielectric loss (and, thus, high quality factor Q) leading to a favorable tunability×Q figure of merit (FOM). Advances in obtaining higher film quality and domain engineering have led to an ongoing increase in tunability and FOM values over the past several decades (Fig. 1a) and larger surpass commercially available p-n-junction-based varactors. In particular, a high tunability of 13:1 with low loss ( $\tan \delta < 0.001$ ) was obtained for Ba<sub>0.8</sub>Sr<sub>0.2</sub>TiO<sub>3</sub> (BST80) films on SmScO<sub>3</sub> (110) (SSO) substrates possessing interdigitated capacitor (IDC) electrodes due to the presence of domains with polarization oriented in the plane of the film, with the unusual response being attributed to domain-wall fluctuations<sup>14</sup>. Although these results and other recent work<sup>15,16</sup> suggest that domain engineering is a powerful approach for improving functionality, this approach for achieving high tunability remains largely underdeveloped and still shows some drawbacks. For example, the effect of different domain configurations involving both domains with in-plane and out-of-plane polarization (e.g., c/a domains) has not been explored. Additionally, the use of IDC electrodes is unfavorable for practical application because it requires complex device fabrication as well as the application of a high voltage (> 100 V) to obtain high tunability. By contrast, thin films with electrodes in a parallel plate capacitor configuration enable the application of large electric fields with small voltages.

## Results

Here, we explore the dielectric response tunability of 200-nm-thick BST80 films grown on SSO (110) substrates in a parallel plate-capacitor geometry that contain a dense collection of c/a domains with 90° domain walls. Landau-Ginzburg-Devonshire (LGD) calculations (Supplementary S1) show that a very high tunability can be obtained for this system, and experimentally we obtain a colossal tunability of 100:1 at ~15 V and a moderate dielectric loss (Figs. S4 and S5) that leads to a Q of ~100 over the range of ~200 to ~20 kV/cm, achieving one and two orders of magnitude improvement for tunability and FOM, respectively, compared to previous state-of-the-art materials (Fig. 1)<sup>13–27</sup>. Both tunability and FOM are considerably larger than those of the best-performing films reported in the literature<sup>13</sup> for the entire range of static E field values. Avoiding the drawbacks of the IDC geometry, the outstanding performance of these films is obtained with application of low voltages of ~15 V for devices obtained using a facile process, see Supplementary S2.

The LGD model-calculated temperature-strain phase diagram of BST80 (Methods, Fig. 2a, Fig. S8) shows that BST80 exhibits several domain-wall variants and boundaries between those variants that can be accessed by epitaxial strain arising from depositing BST80 on the appropriate substrates with different lattice parameters (and therefore lattice mismatch). A material controlled to be at or near such boundaries is likely to exhibit high dielectric permittivity and tunability. In particular, the LGD calculations show that a tunability of 28:1 can be obtained at ~500 kV/cm for the c/a-domain state obtained for a misfit strain of 0% (Fig. 2b), suggesting that c/a-domain rich films with misfit strain close to zero should exhibit very high tunability.

Based on the guidance from LGD, BST80 films were grown on 20-nm-thick Ba<sub>0.5</sub>Sr<sub>0.5</sub>RuO<sub>3</sub> (BSRO) electrode layers deposited on SSO (110) substrates, corresponding to a misfit strain of 0.1% (Methods). Confirming the LGD prediction, piezoresponse force microscopy (PFM) measurements reveal that the BST80/BSRO/SSO (110) heterostructures exhibit an c/a-domain state with domain periodicity of 188 nm (Fig. S9). X-ray diffraction patterns and the reciprocal space mapping (RSM) studies of the BST80/BSRO/SSO (110) heterostructures (Figs. S10 and S11) show that the reflection from the BST80 is well-aligned with that from SSO, indicating that the film is lattice-

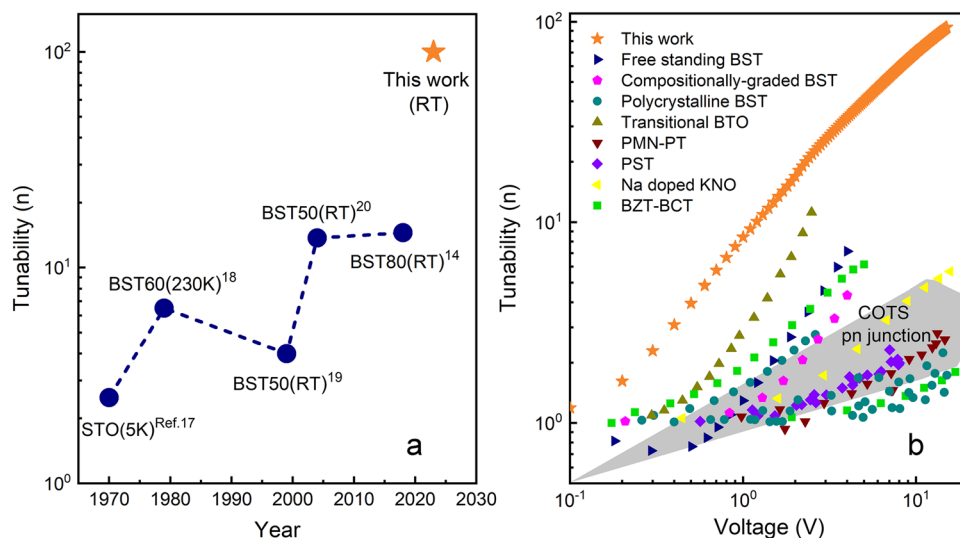


**Fig. 1 | Bias-dependent dielectric tunability and figure of merit in domain-engineered ferroelectric thin films.** **a** Fifty years of progress in enhancing the tunability of Ba<sub>1-x</sub>Sr<sub>x</sub>TiO<sub>3</sub> (0 < x < 1) (BST) -based films (temperature denoted in each)<sup>14,18–20</sup>, including SrTiO<sub>3</sub> (STO)<sup>17</sup> and the present domain-engineered Ba<sub>0.8</sub>Sr<sub>0.2</sub>TiO<sub>3</sub> (BST80) thin films measured at room temperature (RT). **b** Applied static bias field-dependent dielectric tunability for the best-performing domain

wall-engineered BST80 film, in comparison with previously reported Ba<sub>1-x</sub>Sr<sub>x</sub>TiO<sub>3</sub> (0 < x < 1) (BST), BaTiO<sub>3</sub> (BTO), Pb(Mg<sub>1/3</sub>Nb<sub>2/3</sub>)O<sub>3</sub>-PbTiO<sub>3</sub> (PMN-PT), Pb<sub>1-x</sub>Sr<sub>x</sub>TiO<sub>3</sub> (0 < x < 1) (PST), Na doped KNbO<sub>3</sub> (KNO), Ba(Ti<sub>0.8</sub>Zr<sub>0.2</sub>)O<sub>3</sub>-(Ba<sub>0.7</sub>Ca<sub>0.3</sub>)TiO<sub>3</sub> (BZT-BCT) films and Commercial-Off-The-Shelf (COTS) p-n junction varactors (the grey shaded area) in the 1 kHz–100 kHz range<sup>13,15,16,21–27</sup>.

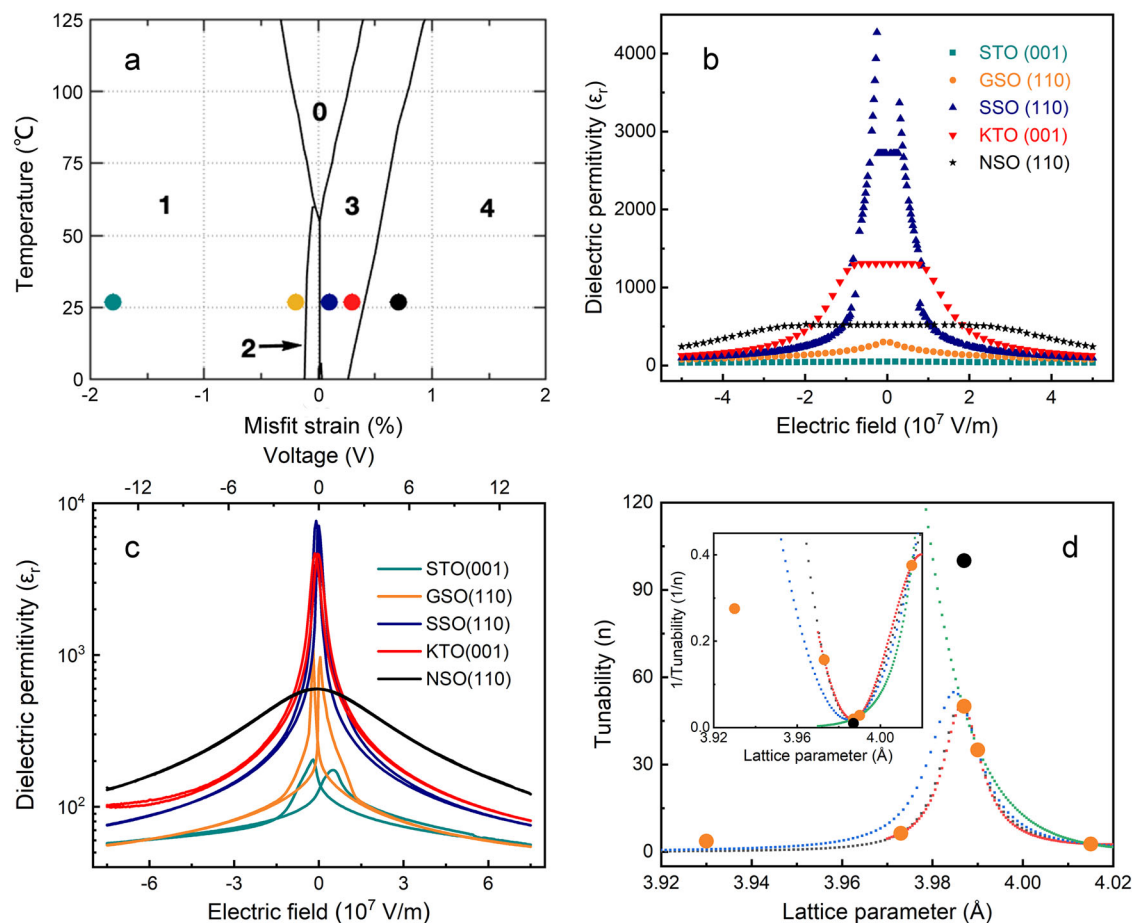


**Fig. 2 | Strain-driven domain engineering for tailoring dielectric tunability.** **a** Landau-Ginzburg-Devonshire (LGD) model-calculated temperature-strain phase diagram of the film plane-normal polarization and domain-wall variants in poly-domain BST80 thin films. Arabic numerals denote various thermodynamically predicted domain structures (see Fig. S8). The dots correspond to the expected strain of BST80 coherently strained on SrTiO<sub>3</sub>(STO)(100), GdScO<sub>3</sub>(GSO)(110), SmScO<sub>3</sub>(SSO)(110), KTaO<sub>3</sub>(KTO)(100), and NdScO<sub>3</sub>(NSO)(110) (from left to right). **b** LGD model-calculated out-of-plane dielectric permittivity for BST80 films under

different strains corresponding to selected substrates. **c** Measured dielectric permittivity, at 10 kHz, of the BST80 films grown on Ba<sub>0.5</sub>Sr<sub>0.5</sub>RuO<sub>3</sub>(BSRO) or SrRuO<sub>3</sub>(SRO)-electroded NSO(110), KTO(100), SSO(110), GSO(110) and STO(100) substrates. **d** Tunability data from **c**, plotted as a function of the BST80 film in-plane lattice parameter described in the Methods section. The inset shows inverse tunability data. The black dots denote the tunability for the BST80/SSO under 100 mV AC bias. Dotted lines indicate fits to the data.

matched to the substrate. Consistent with the PFM results, satellite peaks observed in the RSMs also confirm the presence of domain structures with -188 nm periodicity (Fig. S12).

To examine the effect of strain on the dielectric response and tunability, BST80 films were also deposited on SrTiO<sub>3</sub> (STO) (001), GdScO<sub>3</sub> (GSO) (110), KTaO<sub>3</sub> (KTO) (001), and NdScO<sub>3</sub> (NSO) (110) substrates with BSRO or SrRuO<sub>3</sub> (SRO) bottom and top electrodes, corresponding to misfit strains of -1.8%, -0.2%, 0.3%, and 0.7%, respectively. Similar to the BST80/BSRO/SSO (110) heterostructures, epitaxial growth is obtained for films grown on all substrates and the films grown on GSO, SSO, NSO, and KTO are coherently strained to the substrates, while the films grown on STO are relaxed (Figs. S10 and S11). The measured ferroelectric polarization-electric field hysteresis loops for all heterostructures (Fig. S13) show that the BST80/BSRO/NSO (110) exhibits essentially dielectric behavior, indicating that the switchable out-of-plane polarization is effectively zero for this tensile-strain condition. By contrast, wide loops consistent with strong out-of-plane polarization are obtained for the BST80/BSRO/GSO (110) and BST80/SRO/STO (001) heterostructures wherein there is compressive strain on the films. The BST80/BSRO/SSO (110) and BST80/BSRO/KTO (001) heterostructures with a slight strain exhibit similar slender hysteresis loops

with a high slope at the origin. This suggests that the most sensitive dielectric response will be obtained for the BST80/BSRO/SSO (110) and BST80/BSRO/KTO (001) heterostructures.

Dielectric measurements confirm that the location of the heterostructure in the temperature-strain phase diagram profoundly affects its static bias-dependent dielectric response (Fig. 2c and Fig. S14). The BST80/SRO/STO and BST80/BSRO/NSO heterostructures, on the two opposite sides of the phase diagram, show the least tunability, with the tunability increasing toward the center of the phase diagram and reaching high values for the BST80/BSRO/SSO (110) and BST80/BSRO/KTO (001) heterostructures. While the dielectric constant values of the BST80/BSRO/SSO (110) and BST80/BSRO/KTO (001) heterostructures are essentially the same, the tunability of the BST80/BSRO/SSO (110) heterostructures is greater than that of the BST80/BSRO/KTO (001) heterostructures due to the stronger suppression of the dielectric response by the applied static bias.

Examination of the tunability as a function of the film in-plane lattice parameter reveals a peak in the vicinity of  $a = 3.99$  Å (Fig. 2d). Such peaks in the response properties are typically found at (or near) phase boundaries where the flattening of the potential energy surface makes the system extremely sensitive even to a weak perturbation

due to the inverse relationship between the potential energy surface curvature and the magnitude of the response property. One example of this is the peak in the piezoelectric response with respect to composition found at the morphotropic phase boundary (MPB) in piezoelectrics such as lead zirconate titanate and lead magnesium niobate-lead titanate due to the flattening of the polarization rotation potential energy surface across the MPB. Since our BST80/BSRO/SSO films are located close to the phase boundary, a small perturbation of the system by the change of the in-plane lattice parameter from that of KTO (001) to that of SSO (110) gives rise to a large change in the response of the material. This is illustrated in the plot of inverse tunability versus lattice strain that shows a very small difference in the inverse tunability between BST80/BSRO/KTO (001) and BST80/BSRO/SSO (110) heterostructures (Fig. 2d, inset) that translates into a large enhancement of the tunability from 35:1 to 50:1. Thus, this begs the question whether a tunability even higher than 50:1 may be obtained for BST80/BSRO/SSO (110) heterostructures by further fine-tuning of the system. To achieve higher tunability, we investigate the use of different electrode-ferroelectric interfaces and amplitude modulation of the measurement bias as additional knobs for the fine-tuning of the BST80/BSRO/SSO (110) system beyond lattice-mismatch strain.

Since it is well-known that the properties of ferroelectric capacitors can depend on the metal-ferroelectric electrostatic barrier and its interfacial quality<sup>28</sup>, we explored different top electrode materials (Au/Ti, Pt/Ti, BSRO deposited at room temperature (RTBSRO), BSRO deposited at high temperature (HTBSRO)) for the modification of the BST80 film system. Top  $90\ \mu\text{m} \times 90\ \mu\text{m}$  20-nm-thick electrodes were lithographically patterned on the BST80 films using a water-soluble hard mask process adapted from ref. 29 (Methods and Supplementary Information). BSRO-electroded films deposited at high temperature (HTBSRO) exhibited well-defined ferroelectric hysteresis loops and the lowest leakage currents (Fig. 3a, b). Dielectric measurements of the films reveal a strong sensitivity of the dielectric response to the variation in the electrode-ferroelectric interface and applied bias voltage (Fig. 3c). For all heterostructure-electrode pairs, the relative dielectric permittivity ( $\epsilon$ ) decreases rapidly with applied bias, with the magnitude of the zero-field permittivity and its changes under bias going from smallest to largest in the order of Au/Ti < Pt/Ti < RTBSRO < HTBSRO, with  $\epsilon = 4700$  reached for the HTBSRO-electroded films. Remarkably, the HTBSRO-electroded films show a two-fold increase in the zero-field  $\epsilon$  relative to the RTBSRO film, and four-fold relative to the Pt/Ti films. Upon the application of a static bias,  $\epsilon$  decreases to as low as 76, demonstrating the exceptional tunability of these films.

Thus, the changes in the electrode-ferroelectric interface can be used to enhance the dielectric response of the BST80/SSO (110) system.

Variation of the modulation amplitude of the measurement bias is another method for fine-tuning the domain-rich BST80/BSRO/SSO (110) films to obtain a large enhancement of the dielectric response. Since the tunability of our films is predicted by LGD to be due to the changes in the domain structure (or domain fractions) under applied field, the kinetics of domain-wall motion are likely to be important, and domain-variant fractions should be highly sensitive to the applied electric field due to small energy differences and kinetic barriers between the different domain-wall variants, with larger modulation amplitude expected to increase the response. Experimentally, larger values of the dielectric constant are indeed obtained for a higher amplitude modulation of the measurement bias at low static bias voltage for the heterostructures (Fig. 4a and Fig. S6) with more than two-fold enhancement in the dielectric constant of the BST80/BSRO/SSO (110) heterostructures, reaching  $\epsilon = 8400$ . The enhancement decays rapidly as static bias is applied and disappears at the bias magnitude of  $-40\ \text{kV/cm}$  (or  $30\ \text{kV/cm}$ ) as the system moves away from the phase boundary and the kinetic barriers for domain-wall motion increase. The kinetic effect leads to an enhancement in the tunability, with the tunability reaching 72:1 for an amplitude modulation of 10 mV and 100:1 for 100 mV. The peak dielectric permittivity and tunability at zero static bias are observed at the modulation amplitude of 230 mV (Fig. 4b) for the BST80/BSRO/SSO and BST80/BSRO/KTO heterostructures. As discussed in the Supplementary Information, this effect can be explained by the higher speed of domain switching and domain-wall motion at higher applied modulation amplitude. This is true, however, only at zero DC bias and low applied modulation amplitude where the system is close to the phase boundary and the response is dominated by domain-wall motion. At higher DC bias and high applied modulation amplitude, the system moves away from the domain-phase boundary, and the dielectric response is increasingly dominated by the standard increase of intrinsic material polarization under applied field.

Achieving temperature independence of tunability is another key consideration for tunable dielectric materials, and naturally, the question of the effect of proximity to theoretically calculated domain-wall-variant boundaries in the epitaxial strain-temperature phase diagram on film properties arises. Dielectric measurements were performed to examine the temperature dependence of the tunability and dielectric loss of the BST80/BSRO/SSO (110) heterostructures (Fig. 4c). At  $50\ ^\circ\text{C}$ , the tunability reaches as high as 100:1 for 100 mV, which is the highest

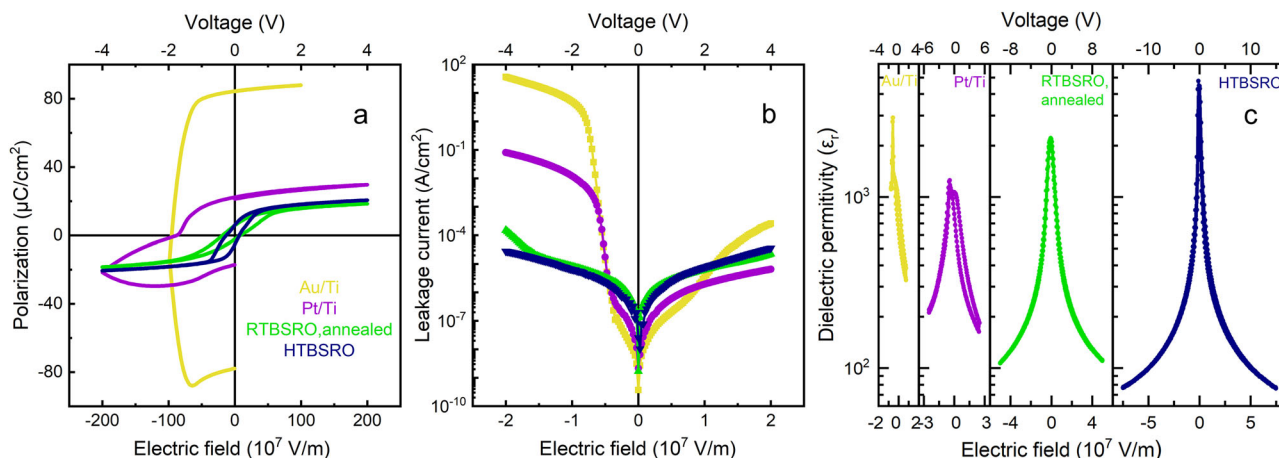


**Fig. 3 | Ferroelectric and dielectric behavior engineered by top electrodes of BST80 films.** **a** Polarization-voltage traces, **b** leakage current, and **c** bias-dependent dielectric permittivity of BST80/SSO capacitors with Au/Ti, Pt/Ti, room

temperature deposited BSRO (RTBSRO), and high temperature deposited BSRO (HTBSRO) top electrodes collected at 10 kHz.



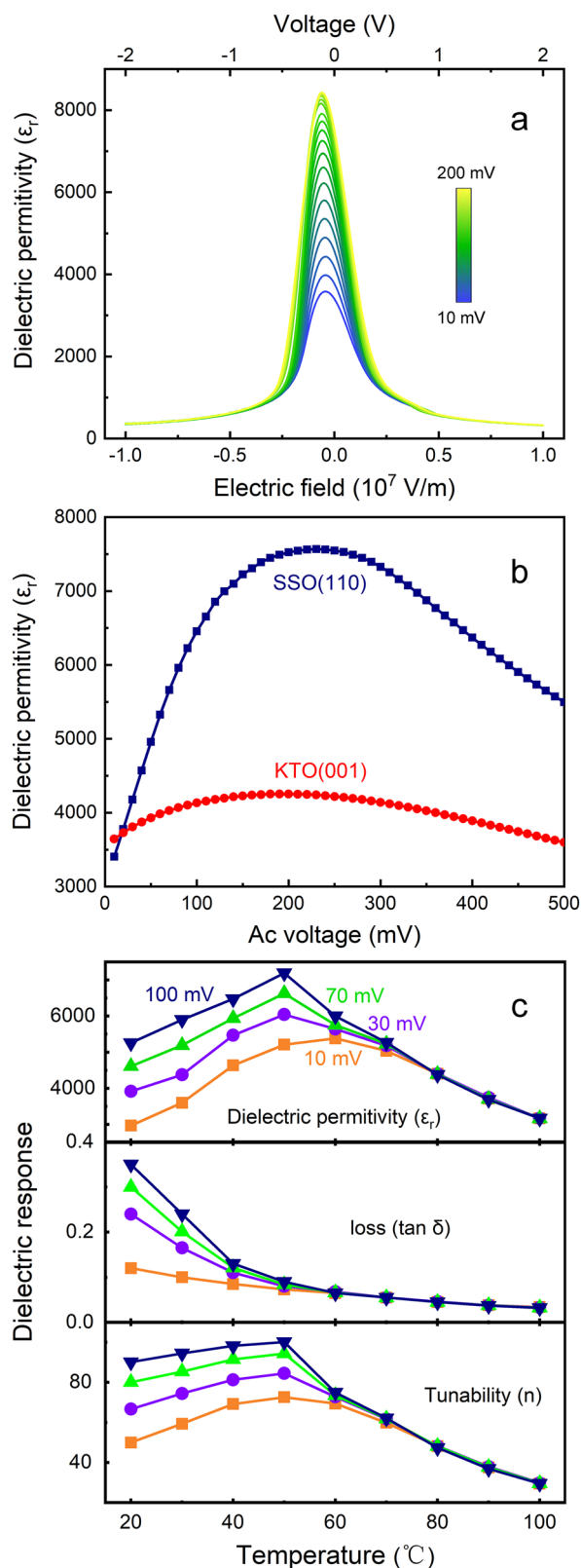


**Fig. 4 | Variation of dielectric permittivity and tunability of BST80 films with modulation amplitude of measurement bias.** **a** Static bias field dependence of the dielectric permittivity of a BSRO/BST80/BSRO/SSO capacitor collected with various modulation amplitudes of measurement voltage. **b** Dielectric permittivity of the BSRO/BST80/BSRO/SSO and BSRO/BST80/BSRO/KTO capacitors as function of modulation amplitude, collected at zero static bias voltage. **c** Temperature dependence of the dielectric permittivity, loss and tunability of BSRO/BST80/BSRO/SSO capacitor measured at different modulation amplitudes as denoted.

tunability reported to date to the best of our knowledge and is approximately an order of magnitude higher than that in IDC films on SSO<sup>14</sup>. As the system moves away from the phase boundary with increasing temperature, the tunability decreases but is still quite high (30:1 at 100  $^{\circ}\text{C}$ ), surpassing the performance of films previously reported<sup>15,16,21–27</sup>. Contrary to the observed high sensitivity of the tunability to epitaxial strain (Fig. 2c), the temperature dependence of the tunability and dielectric loss is comparable to previous reports<sup>13</sup>.

## Discussion

For all modulation amplitude values, the peak dielectric constant is obtained at 50  $^{\circ}\text{C}$  and the dielectric constant becomes independent of the modulation amplitude at  $T > 70$   $^{\circ}\text{C}$ , corresponding to the temperature of the peak dielectric constant obtained from dielectric measurements (Fig. S16). Above this temperature the barriers to domain-wall motion become small and the response becomes independent of bias because the response of the system to the applied field is essentially instantaneous and therefore is governed purely by thermodynamics. Below 70  $^{\circ}\text{C}$ , domain-wall motion gives rise to a larger dielectric response that is kinetically dependent and therefore enhanced by application of larger measurement bias. As expected from the exponential dependence of the domain-nucleation energy on the inverse electric field-temperature product ( $ET$ )<sup>-1</sup><sup>30–32</sup>, the dielectric constant enhancement by higher applied alternating current (AC) measurement bias increases with lower temperature. The dielectric loss is  $\approx 0.02$  ( $Q \approx 50$ ) for  $T > 50$   $^{\circ}\text{C}$  and then increases with decreasing temperature, with greater increase observed for higher applied AC measurement bias. This is expected because domain-wall motion typically leads to greater loss for ferroelectric films. The highest product of tunability and loss is obtained at 50  $^{\circ}\text{C}$ , with a giant tunability of 100:1 and  $Q$  of 50 at 0 V and an excellent tunability of 6:1 with  $Q > 100$  at room temperature over the range of  $-200$  to  $-20$  kV/cm (Fig. S5).

The ability to dynamically modulate the tunability itself simply by changing the amplitude of the measurement bias modulation is a powerful tool for design of devices such as varactors and phase shifter. Current varactors require application of bias voltages, operating over a range of several to tens of V or higher for power-hungry components. The ability to tune the capacitance of a dielectric using modulation only with no dc bias enables varactor functionality at a small fraction ( $\sim 5\%$ ) of the power consumption of current varactors, opening new avenues for highly energy-efficient analog electronics, including sensors, amplifiers, and tuners. Similarly, the ability to tune the capacitance continuously using modulation of AC bias only enables design of a continuous phase shifter with a much simpler design than the current shifters that can only provide discrete phase shifts. We anticipate that the combination of low bias voltage, flexibility of electrode-ferroelectric interface engineering, facile fabrication and measurement voltage amplitude modulation for optimization and control of film dielectric properties and the outstanding performance of these films make domain wall-engineered films promising for further development and use in a variety of novel devices.

## Methods

### SrRuO<sub>3</sub>/Ba<sub>0.5</sub>Sr<sub>0.5</sub>RuO<sub>3</sub> buffered Ba<sub>0.8</sub>Sr<sub>0.2</sub>TiO<sub>3</sub> thin films growth and top electrodes preparation

Single crystal SmScO<sub>3</sub> (110), NdScO<sub>3</sub> (110), GdScO<sub>3</sub> (110), KTaO<sub>3</sub> (001) and SrTiO<sub>3</sub> (STO) (001) substrates were employed for the deposition of 200 nm-thick Ba<sub>0.8</sub>Sr<sub>0.2</sub>TiO<sub>3</sub> thin films with KrF excimer laser (COMPExPro 205). The deposition recipe involves a laser fluence of 2.43 J/cm<sup>2</sup>, a pulse frequency of 2 Hz, and an

oxygen pressure of 100 mTorr at a temperature of 600 °C. In order to reduce the lattice mismatch strain, 20 nm thick SrRuO<sub>3</sub> bottom electrodes were deposited on the SrTiO<sub>3</sub> with a laser fluence of 1.6 J/cm<sup>2</sup>, a pulse repetition of 10 Hz, and an oxygen pressure of 75 mTorr at 650 °C. 20 nm thick Ba<sub>0.5</sub>Sr<sub>0.5</sub>RuO<sub>3</sub> bottom electrodes were deposited on the SmScO<sub>3</sub> with a laser fluence of 1.9 J/cm<sup>2</sup>, a pulse repetition of 1 Hz, and an oxygen pressure of 20 mTorr at 775 °C. With the assistance of a Sr<sub>3</sub>Al<sub>2</sub>O<sub>6</sub> (SAO) hard mask (see Supplementary S2), top island-like epitaxial SrRuO<sub>3</sub>/Ba<sub>0.5</sub>Sr<sub>0.5</sub>RuO<sub>3</sub> electrodes with a thickness of 20 nm were deposited using the same recipe as the bottom electrodes, except for the deposition temperature of 600 °C to protect the crystallinity of the underlying Ba<sub>0.8</sub>Sr<sub>0.2</sub>TiO<sub>3</sub> thin films. A standard photolithography process was employed for the preparation of the other types of electrodes with thickness of 20 nm, which were deposited on the patterned bilayer photoresists (S1818/LOR 3A, Kayaku) at room temperature. Among these electrodes, the SrRuO<sub>3</sub>/Ba<sub>0.5</sub>Sr<sub>0.5</sub>RuO<sub>3</sub> were deposited by pulsed laser deposition with the same recipe of epitaxial SrRuO<sub>3</sub>/Ba<sub>0.5</sub>Sr<sub>0.5</sub>RuO<sub>3</sub> deposition except the depositing temperature. The Au/Ti and Pt/Ti electrodes were deposited by magnetron sputtering (Denton Explorer 14). After the top electrodes deposition, the photoresists were stripped in N-Methyl-2-pyrrolidone solvent at 65 °C.

### Thin film surface morphology and domain structure characterization

Topographic-height scanning probe microscopy (SPM) was employed to determine the feature at the edge of the SrRuO<sub>3</sub>/Ba<sub>0.5</sub>Sr<sub>0.5</sub>RuO<sub>3</sub> electrodes and the SAO hard mask using SPM probes (RTESPA) in standard intermittent contact mode under ambient. The domain patterns in Ba<sub>0.8</sub>Sr<sub>0.2</sub>TiO<sub>3</sub> thin films grown on SmScO<sub>3</sub>(110) and SrTiO<sub>3</sub>(001) substrates were first identified by piezoresponse force microscopy with Pt-coated probes (SCM-PIC) at a contact resonance frequency of 240 kHz. Reciprocal space mapping (Malvern Panalytical Empyrean 3) was further conducted to investigate the domain structure of the films using a hybrid 2-bounce primary monochromator on the incident beam side and a PIXcel<sup>3D</sup> position-sensitive detector.

### Ferroelectric and dielectric properties measurements

All types of top electrodes possess a square pattern with a side length of 90 μm for probe landing in the electrical measurement. A Precision Multi Ferroic II tester (Radiant Technologies) was employed to conduct the measurement of polarization-electric field hysteresis loops at various frequencies, voltage-pulse-enabled polarization switching, polarization fatigue and retention at different temperatures. Due to the existence of asymmetric electric field in some films, the coercive field  $E_c$  was defined as the value of  $(|E_{c-}| + |E_{c+}|)/2$ , where the  $E_{c-}$  and  $E_{c+}$  denote the negative and positive coercive electric field extracted from the hysteresis loops. A semiconductor characterization system (Keithley 4200-SCS) was used to collect the leakage current data of the films with different top electrodes. In addition, a Model 4210-CVU installed in the Keithley instrument was employed to conduct the dielectric measurements. Specifically, an AC test signal (10 mV RMS to 100 mV RMS) was used a DC voltage bias ranging from -15 V to +15 V to collect the capacitance and dielectric loss of the Ba<sub>0.8</sub>Sr<sub>0.2</sub>TiO<sub>3</sub> thin film capacitors. The dielectric permittivity  $\epsilon_r$  values of the capacitors obtained under bias electric field were obtained using the formula of  $\epsilon_r = \frac{Ct}{\epsilon_0 A}$ , and  $E = \frac{V}{t}$ , where the  $C$  is measured capacitance,  $t$  is the thickness of Ba<sub>0.8</sub>Sr<sub>0.2</sub>TiO<sub>3</sub> thin film,  $\epsilon_0$  is vacuum permittivity, and  $A$  is top electrode area. To elucidate the dependence of tunability on the in-plane lattice parameter of the BST80 film, the functional forms and corresponding fitting parameters used for the curves in Fig. 2d are detailed below. All fits follow a polynomial model of the form

$\frac{1}{y} = \sum a_n x^n$ . Black curve:  $\frac{1}{y} = a_0 + a_1 x + a_2 x^2 + a_3 x^3$ , with fitting coefficients:  $a_0 = 5.3924 \times 10^5$ ,  $a_1 = -4.0315 \times 10^5$ ,  $a_2 = 1.0046 \times 10^5$ ,  $a_3 = -8344.7$ . Red curve:  $\frac{1}{y} = a_0 + a_1 x + a_2 x^2 + a_3 x^3 + a_4 x^4$ , with fitting coefficients:  $a_0 = -6.7528 \times 10^7$ ,  $a_1 = 6.7869 \times 10^7$ ,  $a_2 = -2.5558 \times 10^7$ ,  $a_3 = 4.2774 \times 10^6$ ,  $a_4 = -2.6845 \times 10^5$ . Blue curve:  $\frac{1}{y} = a_0 + a_1 x + a_2 x^2 + a_3 x^3$ , with fitting coefficients:  $a_0 = 6260.2$ ,  $a_1 = -3142.1$ ,  $a_2 = 394.32$ ,  $a_3 = -0.0098899$ . Green curve:  $\frac{1}{y} = a_0 + a_1 x + a_2 x^2 + a_3 x^3 + a_4 x^4 + a_5 x^5 + a_6 x^6$ , with fitting coefficients:  $a_0 = 1.0392 \times 10^{11}$ ,  $a_1 = -1.5757 \times 10^{11}$ ,  $a_2 = 9.9547 \times 10^{10}$ ,  $a_3 = -3.3539 \times 10^{10}$ ,  $a_4 = 6.3559 \times 10^9$ ,  $a_5 = -6.4237 \times 10^8$ ,  $a_6 = 2.705 \times 10^7$ . The results for the temperature dependence of  $P$  and  $E_c$  for BST80/BSRO/SSO and BST80/BSRO/KTO, temperature-dependent P-E loops for BST80/BSRO/KTO, and temperature-dependent zero-field  $\epsilon$  for BST80/SRO/STO, BST80/BSRO/GSO, BST80/BSRO/KTO, BST80/BSRO/NSO are presented in the Supplementary S9.

### LGD modeling

The theoretical predictions of the equilibrium phase and domain structures of Ba<sub>0.8</sub>Sr<sub>0.2</sub>TiO<sub>3</sub> are derived with a computational model based on the Landau-Ginsburg-Devonshire (LGD) thermodynamic approach. The LGD model can be used in two different configurations, either as a single domain model (SD) or a multiphase/polydomain model (MPPD).

The derivation of the SD model follows closely the approach outlined by Shirokov et al.<sup>33</sup>. In the model, the energy of the system is expressed in terms of two independent variables (average strain and average electric field) and a dependent variable (electric polarization). The system state is specified by the fixed values of the strain and the electric field, with the polarization always assuming the value that minimizes the overall system energy. The net energy of the film is a weighted average of the energies of the individual end members of the solid solution with the volume fraction of each end member serving as the weighting factor. The chemical composition of the solid solution is assumed to be uniform throughout the film.

In the polydomain configuration, the thermodynamic state of the system is represented by a combination of two ferroelectric domains separated by a domain wall. The two domains and the corresponding boundary form a regular periodic pattern throughout the material. The energy of the MPPD system is calculated with the model derived similarly to the model described by Koukhar et al.<sup>34</sup>. The Koukhar polydomain model used an infinitesimally thin boundary, while the MPPD model in this analysis uses finite-width domain wall.

The LGD physical constants for BaTiO<sub>3</sub> and SrTiO<sub>3</sub> are taken from<sup>33</sup>, gradient and flexoelectric constants are taken from<sup>35</sup> and<sup>36</sup>, respectively. The dielectric tensor is calculated with a novel method employing the LGD energy functional and a finite-difference approach as described in the Supplementary S1.

### Data availability

Source data are provided with this paper (ref. 37).

### References

- Al-Shetwi, A. Q. Sustainable development of renewable energy integrated power sector: Trends, environmental impacts, and recent challenges. *Sci. Tot Environ.* **822**, 153645 (2022).
- Rabaia, M. K. H. et al. Environmental impacts of solar energy systems: A review. *Sci. Tot Environ.* **754**, 141989 (2021).
- Atawi, I. E., Al-Shetwi, A. Q., Magableh, A. M. & Albalawi, O. H. Recent Advances in Hybrid Energy Storage System Integrated Renewable Power Generation: Configuration. *Control, Appl., Future Directions. Batteries* **9**, 29 (2023).
- Noras, M. A. Electric field sensor based on a varactor diode/MIS/MOS structure, in *2010 IEEE Ind. Appl. Soc. Annu. Meeting*, (2010).

5. Lee, C. H. et al. Exploiting dimensionality and defect mitigation to create tunable microwave dielectrics. *Nature* **502**, 532–536 (2013).
6. Subramanyam, G. et al. Challenges and opportunities for multi-functional oxide thin films for voltage tunable radio frequency/microwave components. *J. Appl. Phys.* **114**, 191301 (2013).
7. Zhang, H. et al. High tunability and low loss in layered perovskite dielectrics through intrinsic elimination of oxygen vacancies. *Chem. Mater.* **32**, 10120–10129 (2020).
8. Arlt, G., Böttger, U. & Witte, S. Dielectric dispersion of ferroelectric ceramics and single crystals at microwave frequencies. *Ann. Phys.* **506**, 578–588 (1994).
9. York, B. in *Multifunctional Adaptive Microwave Circuits and Systems* (eds Steer, M. & Palmer, W. D.) Ch. 6 (SciTech Publishing, Raleigh, 2006).
10. Wang, Y. L., Tagantsev, A. K., Damjanovic, D. & Setter, N. Giant domain wall contribution to the dielectric susceptibility in BaTiO<sub>3</sub>. *Appl. Phys. Lett.* **91**, 062905 (2007).
11. Tagantsev, A. K., Sherman, V. O., Astafiev, K. F., Venkatesh, J. & Setter, N. Ferroelectric materials for microwave tunable applications. *J. Electroceram.* **11**, 5–66 (2003).
12. Xu, F. et al. Domain wall motion and its contribution to the dielectric and piezoelectric properties of lead zirconate titanate films. *J. Appl. Phys.* **89**, 1336–1348 (2001).
13. Everhardt, A. S. et al. Temperature-independent giant dielectric response in transitional BaTiO<sub>3</sub> thin films. *Appl. Phys. Rev.* **7**, 011402 (2020).
14. Gu, Z. et al. Resonant domain-wall-enhanced tunable microwave ferroelectrics. *Nature* **560**, 622–627 (2018).
15. Pesquera, D. et al. Beyond substrates: strain engineering of ferroelectric membranes. *Adv. Mater.* **32**, 2003780 (2020).
16. Damodaran, A. et al. Large polarization gradients and temperature-stable responses in compositionally-graded ferroelectrics. *Nat. Commun.* **8**, 14961 (2017).
17. Saifi, M. A. & Cross, L. E. dielectric properties of strontium titanate at low temperature. *Phys. Rev. B* **2**, 677–684 (1970).
18. Vendik, O. G. *Ferroelectrics at Microwaves* (in Russian) (Sovetskoye Radio, Moscow, 1979).
19. Padmini, P. et al. Realization of high tunability barium strontium titanate thin films by rf magnetron sputtering. *Appl. Phys. Lett.* **75**, 3186 (1999).
20. Pervez, N. K., Hansen, P. J. & York, R. A. High tunability barium strontium titanate thin films for rf circuit applications. *Appl. Phys. Lett.* **85**, 4451 (2004).
21. Gao, D. et al. All-inorganic flexible Ba<sub>0.67</sub>Sr<sub>0.33</sub>TiO<sub>3</sub> thin films with excellent dielectric properties over a wide range of frequencies. *ACS Appl. Mater. Interfaces* **11**, 27088–27097 (2019).
22. Song, L. et al. Fabrication and dielectric properties of Ba<sub>0.63</sub>Sr<sub>0.37</sub>TiO<sub>3</sub> thin films on SiC substrates. *J. Am. Ceram. Soc.* **97**, 3048–3305 (2014).
23. Cole, M. W. et al. Low dielectric loss and enhanced tunability of Ba<sub>0.6</sub>Sr<sub>0.4</sub>TiO<sub>3</sub> based thin films via material compositional design and optimized film processing methods. *J. Appl. Phys.* **93**, 9218–9225 (2003).
24. Han, F., Hu, Y. & Peng, B. High dielectric tunability with high thermal stability of the (111) highly oriented 0.85Pb(Mg<sub>1/3</sub>Nb<sub>2/3</sub>)–0.15PbTiO<sub>3</sub> thin film prepared by a sol-gel method. *J. Eur. Ceram. Soc.* **41**, 6482–6489 (2021).
25. Zheng, Z. et al. High dielectric tunability of (100) oriented Pb<sub>x</sub>Sr<sub>1-x</sub>TiO<sub>3</sub> thin film coordinately controlled by dipole activation and phase anisotropy. *J. Appl. Phys.* **110**, 124107 (2011).
26. Hao, L. et al. Achieving a high dielectric tunability in strain-engineered tetragonal K<sub>0.5</sub>Na<sub>0.5</sub>NbO<sub>3</sub> films. *npj Comput. Mater.* **7**, 62 (2021).
27. Luo, B. et al. Dielectric tunability properties in (110)-oriented epitaxial 0.5Ba(Ti<sub>0.8</sub>Zr<sub>0.2</sub>)O<sub>3</sub>–0.5(Ba<sub>0.7</sub>Ca<sub>0.3</sub>)TiO<sub>3</sub> thin films prepared by PLD method. *Materials* **13**, 4771 (2020).
28. Karthik, J., Damodaran, A. R. & Martin, L. W. Epitaxial ferroelectric heterostructures fabricated by selective area epitaxy of SrRuO<sub>3</sub> using an MgO mask. *Adv. Mater.* **24**, 1610–1615 (2012).
29. Lu, D. et al. Synthesis of freestanding single-crystal perovskite films and heterostructures by etching of sacrificial water-soluble layers. *Nat. Mater.* **15**, 1255–1260 (2016).
30. Merz, W. J. Domain formation and domain wall motions in ferroelectric BaTiO<sub>3</sub> single crystals. *Phys. Rev.* **95**, 690–698 (1954).
31. Miller, R. C. & Weinreich, G. Mechanism for the sidewise motion of 180° domain walls in barium titanate. *Phys. Rev.* **117**, 1460 (1960).
32. Tybell, T., Paruch, P., Giamarchi, T. & Triscone, J.-M. Domain wall creep in epitaxial ferroelectric Pb(Zr<sub>0.2</sub>Ti<sub>0.8</sub>)O<sub>3</sub> thin films. *Phys. Rev. Lett.* **89**, 097601 (2002).
33. Shirokov, V. B., Yuzyuk, Y. I., Dkhil, B. & Lemanov, V. V. Phenomenological theory of phase transitions in epitaxial Ba<sub>x</sub>Sr<sub>1-x</sub>TiO<sub>3</sub> thin films. *Phys. Rev. B* **79**, 144118 (2009).
34. Koukhar, V. G., Pertsev, N. A. & Waser, R. Thermodynamic theory of epitaxial ferroelectric thin films with dense domain structures. *Phys. Rev. B* **64**, 214103 (2001).
35. Morozovska, A. N., Eliseev, E. A., Glinchuk, M. D., Chen, L. Q. & Gopalan, V. Interfacial polarization and pyroelectricity in anti-ferrodistortive structures induced by a flexoelectric effect and rotostriction. *Phys. Rev. B* **85**, 094107 (2012).
36. Hlinka, J. & Marton, P. Phenomenological model of a 90° domain wall in BaTiO<sub>3</sub>-type ferroelectrics. *Phys. Rev. B* **74**, 104104 (2006).
37. Chen, D. et al. Colossal and Tunable Dielectric Tunability Data sets. *Figshare* <https://doi.org/10.6084/m9.figshare.29844860> (2025).

## Acknowledgements

This research was sponsored by the Army Research Laboratory and was accomplished under Cooperative Agreement Number W911NF-24-2-0100. The views and conclusions contained in this document are those of the authors and should not be interpreted as representing the official policies, either expressed or implied, of the Army Research Laboratory or the U.S. Government. The U.S. Government is authorized to reproduce and distribute reprints for Government purposes notwithstanding any copyright notation herein. This work was also supported in part by the Army Research Office under W911NF-21-1-0126. Y.J. acknowledges that this work was supported by the Air Force Office of Scientific Research under award number FA9550-24-1-0266. Any opinions, findings, and conclusions or recommendations expressed in this material are those of the author(s) and do not necessarily reflect the views of the United States Air Force. This work was carried out in part at the Singh Center for Nanotechnology, which is supported by the NSF National Nanotechnology Coordinated Infrastructure Program under grant NNCI-2025608.

## Author contributions

J.E.S. designed and supervised this study. D.C. and L.W. synthesized the thin films, and D. C. and Y.J. developed the SAO hard mask preparation process. D.C. fabricated the capacitor-based devices, characterized the ferroelectric domain configuration, and performed the various electrical, dielectric, and ferroelectric measurements. S.N. and Z.G. conducted thermodynamic modeling. J.C. and C.J.G.M. measured the GHz-band dielectric tunability. D.C. drafted the initial manuscript, and I.G., K.C., L.W.M. and J.E.S. revised the manuscript. All authors contributed to the discussion and preparation for the final manuscript.

## Competing interests

The authors declare no competing interests.

## Additional information

**Supplementary information** The online version contains supplementary material available at <https://doi.org/10.1038/s41467-025-63449-4>.

**Correspondence** and requests for materials should be addressed to Jonathan E. Spanier.

**Peer review information** *Nature Communications* thanks the anonymous reviewers for their contribution to the peer review of this work. A peer review file is available.

**Reprints and permissions information** is available at <http://www.nature.com/reprints>

**Publisher's note** Springer Nature remains neutral with regard to jurisdictional claims in published maps and institutional affiliations.

**Open Access** This article is licensed under a Creative Commons Attribution-NonCommercial-NoDerivatives 4.0 International License, which permits any non-commercial use, sharing, distribution and reproduction in any medium or format, as long as you give appropriate credit to the original author(s) and the source, provide a link to the Creative Commons licence, and indicate if you modified the licensed material. You do not have permission under this licence to share adapted material derived from this article or parts of it. The images or other third party material in this article are included in the article's Creative Commons licence, unless indicated otherwise in a credit line to the material. If material is not included in the article's Creative Commons licence and your intended use is not permitted by statutory regulation or exceeds the permitted use, you will need to obtain permission directly from the copyright holder. To view a copy of this licence, visit <http://creativecommons.org/licenses/by-nc-nd/4.0/>.

© The Author(s) 2025